

Position and Time Determination without Prior State Knowledge via Onboard Optical Observations of Delta Scuti Variable Stars

Linyi Hou^{1*}, Ishaan Bansal¹, Clark Davis¹, Siegfried Egg1¹

^{1*}Department of Aerospace Engineering, University of Illinois
Urbana-Champaign, 104 S Wright St., Urbana, IL 61820.

*Corresponding author(s). E-mail(s): linyh2@illinois.edu;
Contributing authors: egg1@illinois.edu; ibansal2@illinois.edu;
clarkjd2@illinois.edu;

Abstract

We present a navigation concept for solving the lost in space and time problem using optical observations of δ Scuti variable stars. Only a small number of techniques exist that allow a spacecraft to recover from being lost in both space and time, which can be caused by a failure of the onboard clock and navigation systems. Optical observations of δ Scuti stars, which can be collected onboard from star trackers or navigation cameras, may enable faster and/or more accurate position and time solutions compared to existing techniques without requiring additional equipment. Our results indicate that one day of observation by the OSIRIS-APEX MapCam may enable position and time determination accuracy within 0.05 au (3σ) and 15 s (3σ).

Keywords: Lost in Space, Star Tracker, δ Scuti, Space Navigation

1 Introduction

Onboard knowledge of spacecraft state can become lost or severely outdated due to power or data loss coupled with loss of contact to ground stations on Earth; this is known as the lost in space problem. In such cases, a spacecraft must autonomously take action to recover its state knowledge or reestablish communication.

Most onboard spacecraft command and data handling (C&DH) systems include contingencies for lost in space or similar scenarios. The New Horizons spacecraft has a “Sun Acquisition” mode in which its high-gain antenna is pointed to the Sun to send a signal indicating a critical fault if communication with the Earth cannot be established [1]. The Jupiter Icy Moons Explorer (JUICE) and Rosetta spacecraft both have an “Earth Strobing” mode in which the spacecraft rotates slowly with the medium gain antenna sweeping past Earth each rotation [2, 3]. However, such contingencies for the lost in space scenario ultimately rely on ground stations to provide commands that update the spacecraft state, which has proven difficult in the past. For example, the STEREO-Behind satellite was recovered briefly through extensive search operations conducted using the Deep Space Network (DSN) over 22 days [4]. More recently, Voyager 2 was inadvertently commanded to point its antenna away from the Earth and required signaling from the DSN to correct its attitude [5].

Ground-based tracking and recovery methods rely on spacecraft either being able to receive signals regardless of antenna orientation or being able to point their antenna in the direction of Earth with sufficient accuracy. The former requires a powerful transmitter and proximity to Earth, while the latter may be challenging for interplanetary missions. Furthermore, for deep space missions, ground-based signaling typically relies on the DSN, whose schedule has become overloaded due to the growth in mission demand and data return [6]. In contrast, techniques that allow a spacecraft to autonomously recover its position and time using onboard measurements alone are more scalable as the number of operational spacecraft increases.

While numerous methods have been proposed to solve the lost in space problem using onboard measurements alone (assuming known time) [7–9], only a handful of methods are capable of recovering spacecraft that are lost in both space *and time*. Adams and Peck introduced an optical navigation (OpNav)-based solution applicable within the vicinity of the Earth and Moon [10]. Dahir developed a method using star trackers to observe the Sun, Jupiter, and its moons for navigation between 1 au to 5 au from the Sun [11]. Sala et al. devised a lost in space and time algorithm based on observations of X-ray pulsars [12].

Solutions to the lost in space and time problem that depend on signal sources from within the Solar System have several limitations. The location of those signal sources are highly sensitive to the current time and the observer’s position, which means the observer may need to search the entire sky to find a signal. Additionally, illumination by the Sun and occlusion by nearby planets makes these techniques only applicable in certain parts of the Solar System (such as the vicinity of Earth or within 5 au of the Sun). Signal sources from beyond the Solar System have smaller parallax from temporal and positional changes in the Solar System and can largely mitigate the aforementioned issues. However, the only existing lost in space and time navigation algorithms based on extrasolar sources utilize X-ray pulsars, which are faint and require long observation times with specialized detectors. Additionally, extensive computation is required to perform ambiguity resolution [9].

In this paper, we present a novel solution for autonomous recovery from being lost in both space and time by using onboard observations of δ Scuti variable stars in the optical band. In contrast to existing methods, the proposed technique may be performed almost anywhere in the Solar System within a few hours using a single optical detector such as a star tracker or navigation camera. While the accuracy of our proposed solution is likely insufficient to be used as a standalone navigation technique, it may be used to facilitate other higher accuracy navigation methods that would have

been otherwise infeasible in a lost in space and time scenario. In particular, we believe that our method can be used in combination with on board planetary ephemerides to determine the relative position of the spacecraft with respect to the Earth to sufficient accuracy so as to enable re-acquisition of contact with ground stations.

2 δ Scuti Variable Stars

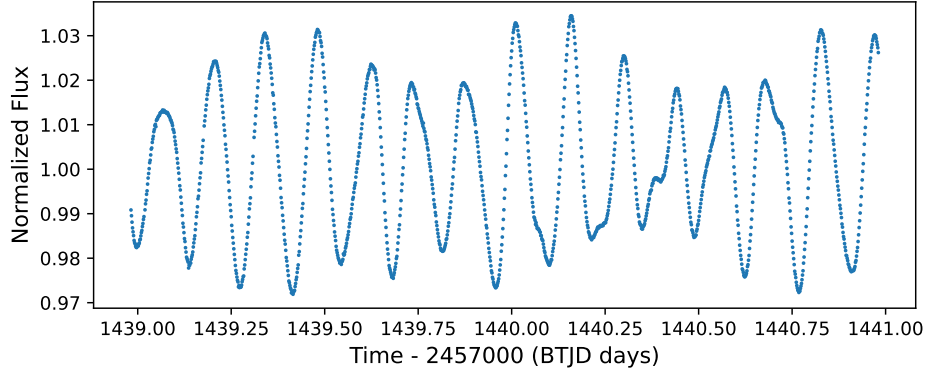
δ Scuti stars are a type of pulsating variable star whose luminosity varies due to the periodic expansion and contraction of the surface layers of the star [13, 14]. Each δ Scuti star’s luminosity variation may comprise many pulsation modes with periods ranging from a few minutes to several hours [15]. Optical detectors such as star trackers and navigation cameras may be used to measure the varying flux of a δ Scuti star. Figure 1 shows the light curve and dominant pulsation frequencies of the δ Scuti star X Caeli as measured by the Transiting Exoplanet Survey Satellite (TESS).

From the International Variable Star Index (VSX) [16], we compiled a list of δ Scuti stars with apparent magnitudes of $m_V < 7.0$ in the Johnson V filter, brightness modulation amplitudes $\Delta V > 0.04$ mag, and modulation periods $P < 0.20$ days. The selection criteria was chosen to allow detectable levels of pulsation within the capabilities of a star tracker or navigation camera. A total of 44 δ Scuti stars met the above criteria and are listed in the appendix, Table A1. While the present analysis exclusively considers δ Scuti stars, the concept may extend to other optical variable stars such as RR Lyrae and Cepheid variables.

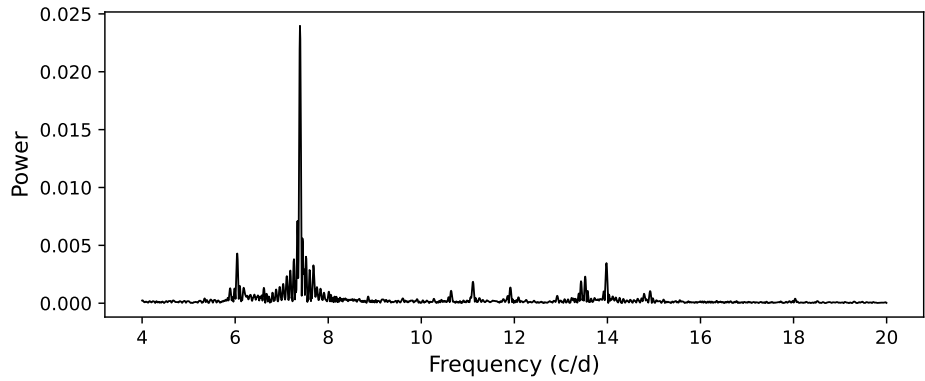
The light curve of a δ Scuti star can be modeled as the sum of its pulsation modes, which in turn can each be modeled as sine waves. The model of a δ Scuti star’s light curve is then:

$$\omega_{\mathbf{b}}(t) = A_0 + \sum_i A_i \cdot \sin(2\pi f_i(t - t_0) + \phi_i) \quad (1)$$

where A_i , f_i , ϕ_i are the amplitude, frequency, and phase offset of each pulsation mode, A_0 is the brightness or magnitude offset, t_0 is the model epoch, and \mathbf{b} is the



(a)



(b)

Fig. 1: Normalized light curve of the δ Scuti star X Caeli (a) and its pulsation spectra (b). The dominant frequencies — 7.392, 6.046, and 13.980 cycles per day — are in close agreement with results from Ref. [17].

reference observatory at which observations are made. The reference observatory is commonly chosen to be the Solar System barycenter (SSB). The proposed lost in space and time navigation algorithm relies on finding $(t - t_0)$, the difference between measurement time and the model epoch, to perform navigation. This is achieved by fitting the measured light curve of a δ Scuti star to its model.

Despite the sum of multiple pulsation modes creating irregularities in the light curve such as those shown in Figure 1a, the light curves of δ Scuti stars are still largely

periodic. Therefore, the measured light curve of a star does not correspond to a unique segment of the pulsation profile. Rather, there are an infinite number of possible values of t which may fit the measurement data. This problem is very similar to the phase ambiguity problem encountered when performing X-ray pulsar navigation [9] and is later addressed in Section 5.2.

3 Detector Characterization

The chosen δ Scuti stars are bright in the V-band and have prominent brightness variations, so they can be observed using optical detectors that are commonly on board spacecraft such as star trackers and navigation cameras. Several optical detector arrangements are listed in Tables 1-2, including commercial star trackers, experimental low-cost star trackers, and instruments from the OSIRIS-REx/APEX camera suite.

Table 1: Camera specifications.

Name	FOV (deg ²)	IFOV (μ rad/px)	Focal Length (mm)	Aperture (mm)
OREx SamCam [18, 19]	20.8×20.8^1	354	24	4.3
OREx MapCam [18, 19]	4.0×4.0^1	68	125	38
OREx PolyCam [18, 19]	0.82×0.82^1	13.5	629	175
OREx NavCam [20]	44×32	280	7.64	2.18
Blue Canyon NST [21]	10×12	170	30.2	-
μ STAR-100M [22]	-	-	50	41.7
Terma T1 [23]	20×20^1	340	-	26
AeroCube [24]	64×36	872	6.3	3.15
MIT [25, 26]	30×24.25	409	15.97	7.5
CubeStar [27, 28]	51.6×27.28	930	6	5

¹circular FOV.

Table 2: Sensor specifications.

Name	Pixel Size (μm^2)	Readout Noise (e^-)	Gain (e^-/ADU)	Dark Current (pA/cm^2)	Quantum Efficiency
OREx OCAMS [18, 19]	6.5×8.5	<50	4.5	0.065	0.3-0.4
OREx NavCam [20]	1.43×1.43	6.7	1	0.05-0.14	<0.62
Blue Canyon NST [29]	5.3×5.3	-	-	-	-
$\mu\text{STAR-100M}$ [22, 30]	18×18	-	-	0.01 @ 0°C	0.35-0.45 ¹
Terma T1 [23, 31]	10×10	21	-	0.279 @ 21°C	0.5-0.6 ¹
AeroCube [24, 26]	5.6×5.6	2.2	-	0.204 @ 21°C	0.55-0.65
MIT [25, 32]	6.7×6.7	39	10	1.46 @ 21°C	0.3 ¹
CubeStar [27, 28]	5.6×5.6	-	2.28	11.74 @ 65°C	-

¹quantum efficiency \times fill factor.

4 Simulated Observations

The present analysis simulates the flux measurement of δ Scuti stars as measured by an orbiting spacecraft. First, δ Scuti star pulsation models are generated by fitting pulsation modes to observation data from TESS. Using X Caeli as an example, pulsation modes shown in Figure 1b with amplitudes greater than 5% of the maximum amplitude are used to construct a reference light curve as shown in Figure 2. Since the generated reference light curves only need to capture the multi-frequency nature of δ Scuti stars rather than recreate their exact behavior, it was deemed unnecessary to incorporate lower amplitude modes. TESS data (and therefore the generated reference light curves) uses the SSB as the reference observatory.

The present study simulates δ Scuti star observations at the detector level. The source flux, background flux, and dark current measured by an optical detector are modeled as independent Poisson distributions. The mean source flux is time varying and equal to the value of the reference light curve at the time of measurement. Changes in the spacecraft position between measurements, as well as light propagation delay between the SSB and the spacecraft, are accounted for. However, stellar aberration, lens distortion, and other effects that impact the apparent position of the star on the imaging sensor are not considered.

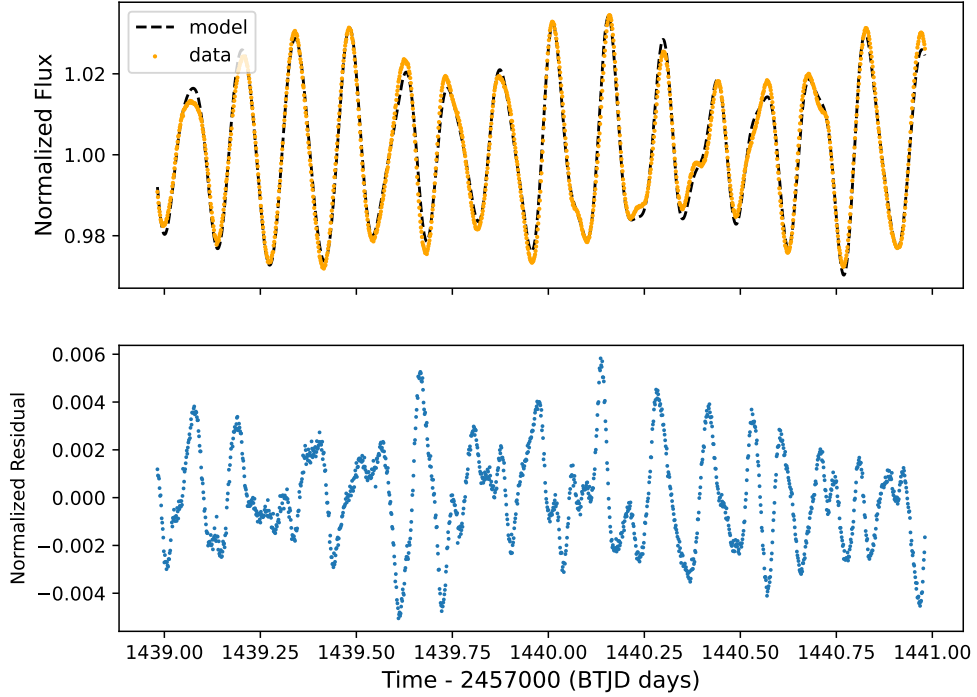


Fig. 2: TESS observation data of X Caeli is used to reconstruct its pulsation model (top panel). The model fit residuals are shown (bottom panel).

The OSIRIS-APEX mission trajectory was selected as a case study. During its cruise to encounter asteroid Apophis in 2029, OSIRIS-APEX will undergo several perihelion passes during which communication with the Earth may not be available. During these times, the ability to autonomously recover from being lost in space and time may be especially important. Figure 3 shows the position of the four inner planets and OSIRIS-APEX on September 2, 2024 during the first perihelion passage.

A subset of 15 δ Scuti stars were arbitrarily selected to be observed. At the selected epoch, only 11 of the stars are visible assuming a 45° Sun exclusion zone for the detector. The visible δ Scuti stars are shown in Figure 4 along with the Solar System planets.

Parameters of the OSIRIS-APEX MapCam instrument are used to simulate δ Scuti observations. It is assumed that the spacecraft will sequentially observe each δ

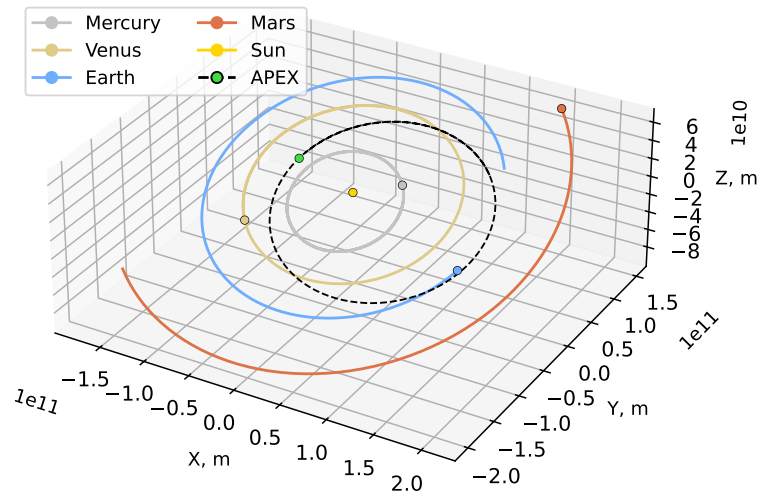


Fig. 3: The positions of the inner planets and OSIRIS-APEX are shown for MJD 60555 (Sep. 2, 2024). OSIRIS-APEX and the Earth are in opposition with respect to the Sun.

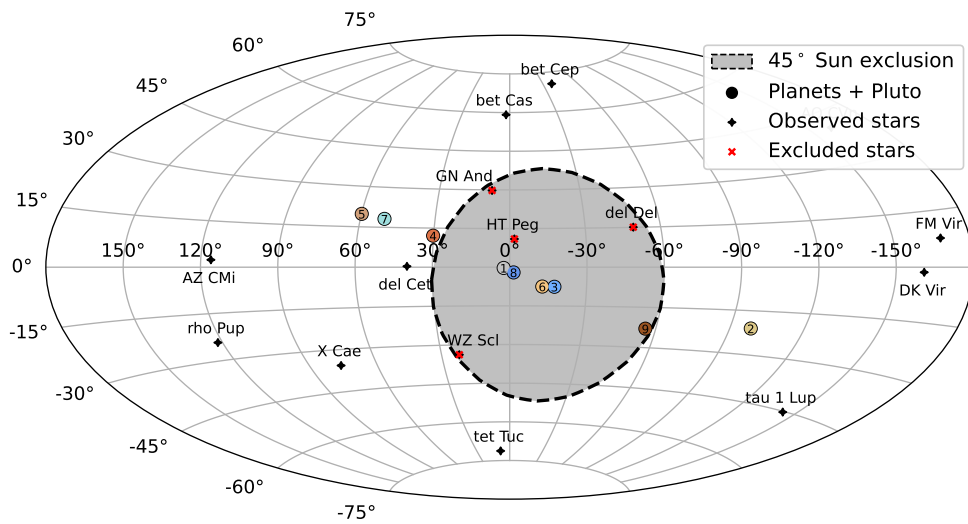


Fig. 4: Distribution of 15 δ Scuti stars and Solar System planets from the view of OSIRIS-APEX used in the analysis are shown in the J2000 equatorial coordinate system using Aitoff projection.

Scuti star for one hour, then repeat the process once after all selected stars have been observed. Images are taken at a 3 s cadence; a 1 min slew time is allotted between observations of different stars. The reference light curves and simulated flux measurements of 11 δ Scuti stars are shown in Figure 5.

Finally, we use the simulated flux measurements to estimate when the signal would arrive at the SSB. For a set of flux measurements $\{S_1, \dots, S_n\}$ at times $\{t_1, \dots, t_n\}$, we find dt which minimizes cost J using gradient descent:

$$J(dt) = \frac{1}{n} \sum_1^n \left(S_i - \omega_{\mathbf{b}}(t_i + dt) \right)^2 \quad (2)$$

To interpret the results, we say that the detector would have measured the same flux S_i at time $(t_i + dt)$ if it were located at the SSB. However, since δ Scuti stars' signals can be highly periodic, there may be an infinite number of local minima for dt depending on the starting point for gradient descent, and they will all be valid estimates of dt . Therefore, the signal time of arrival at the SSB is ambiguous. The navigation algorithm described in the following section addresses the ambiguity resolution problem.

In practice, the spectral sensitivity of the optical detector onboard the spacecraft may be different from the bandpass in which a δ Scuti star's pulsation is modeled. This means that it may be challenging to accurately construct $\omega_{\mathbf{b}}(t)$ to match the sensitivity of a particular detector. It may be possible to address this issue via calibration either in-flight or during instrument qualification, or through the design of a different cost function J ; the present analysis does not consider the impact of this flux modeling error.

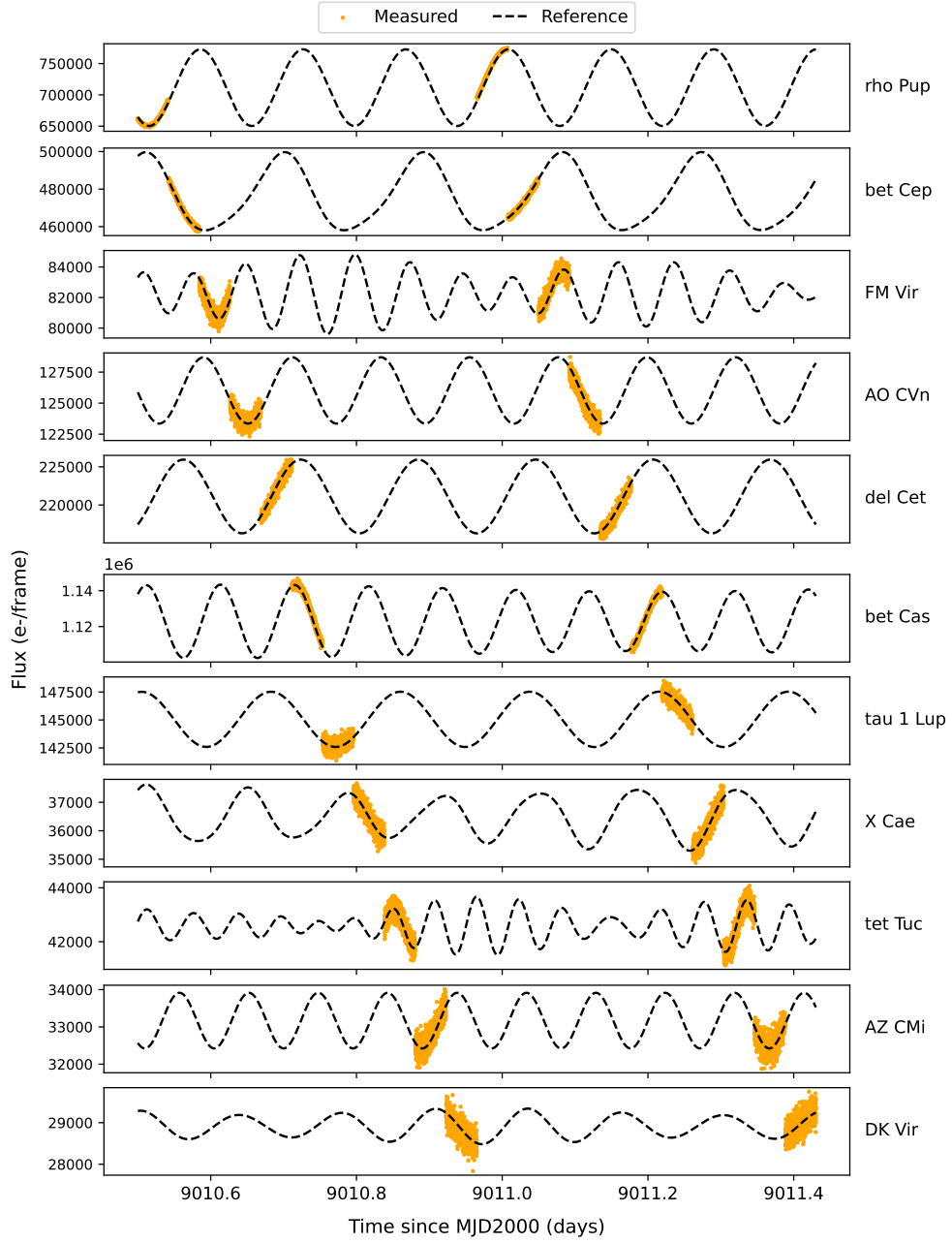


Fig. 5: Reference light curves of 11 δ Scuti variable stars and their simulated flux measurements by MapCam onboard OSIRIS-APEX with 3s exposures.

5 Navigation Algorithm

The lost in space and time navigation algorithm implemented in this paper is comprised of two parts: a linear system to solve for position and time given dt estimates from a set of δ Scuti stars, and a search algorithm to resolve the ambiguity in the value of dt for each star.

Suppose that a spacecraft receives a signal from a δ Scuti star, and at that moment the unknown spacetime coordinate of the spacecraft is $\{\mathbf{x}, t\}$. If the signal would have arrived at the SSB at time T based on the estimation process outlined on the previous section, then $\{\mathbf{x}, t\}$ and $\{\mathbf{x}_{\text{SSB}}, T\}$ must be on the same light cone with slope c whose vertex is at the δ Scuti star. c is the speed of light. Consequently, the set of possible spacetime coordinates for the spacecraft is reduced to the surface of light cone; this concept is illustrated for two-dimensional space in Figure 6.

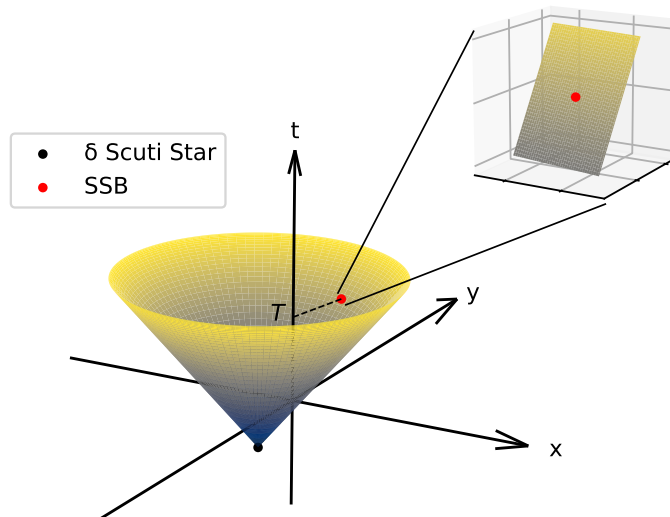


Fig. 6: Illustration of a three-dimensional light cone originating from a δ Scuti star, representing the set of possible spacecraft coordinates given a signal measurement known to pass through the SSB at time T .

For navigation within the Solar System where the length scales involved are far smaller than the distances between the Sun and any δ Scuti star, only a small portion of the light cone around the SSB is relevant. The curvature of the light cone is negligible at the scale of the Solar System, so the set of possible spacecraft spacetime coordinates forms a hyperplane. This is depicted in the enlarged view of the light cone in Figure 6. In similar literature concerning pulsar navigation, these hyperplanes are referred to as “wavefronts”, so we will following the same convention henceforth [12, 33, 34].

Each wavefront represents the possible spacecraft coordinates corresponding to one estimate of dt for a δ Scuti star. However, there are an infinite number of local minima leading to an infinite number of estimates for dt per star. This ambiguity can be resolved by combining observations of multiple δ Scuti stars, since the coordinate of the spacecraft must be at the intersection of the sets of wavefronts. Within a finite spacetime search region, the number of intersections can be reduced to one by observing a large enough number of δ Scuti stars. This concept is illustrated in Figure 7. Note that the figure only illustrates the concept in two dimensions, where each wavefront is a line.

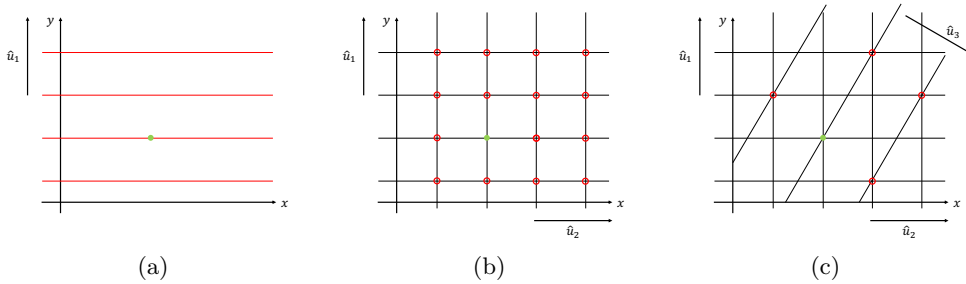


Fig. 7: Two-dimensional example of wavefront intersection. In (a) and (b), the variable star lines of sight are indicated by $\hat{\mathbf{u}}$. The observer’s true spacetime coordinate is in green. The observer’s spacetime coordinate can be on an infinite number of wavefronts — shown in red — when only observing the phase of one variable star (a). Adding wavefronts from observations of other variable stars reduces set of feasible spacetime coordinates to intersections of wavefronts as shown in (b)-(c) [34].

5.1 Closed-form Solution without Ambiguity Resolution

Let there be N δ Scuti stars with known positions on the celestial sphere whose line-of-sight vectors are denoted by $\{\hat{\mathbf{u}}_1, \dots, \hat{\mathbf{u}}_N\}$ in an inertial frame of reference such as the J2000 frame. Assume that a spacecraft whose coordinates are $\{\mathbf{p}, t\}$ measures the light curve of each star and estimates their signals to have arrived at the SSB at T_i for star i . Then the following equation must be satisfied:

$$\hat{\mathbf{u}}_i \cdot \mathbf{p} + c \cdot t = c \cdot T_i. \quad (3)$$

Here, $\{\hat{\mathbf{u}}_i, \mathbf{p}\} \in \mathbb{R}^3$; $\{T_i, t\} \in \mathbb{R}$; and $\|\hat{\mathbf{u}}_i\| = 1$. The relation between \mathbf{p} , \mathbf{b} , and \mathbf{r} is shown in Figure 8. Furthermore, define $\mathbf{r} = \mathbf{p} - \mathbf{b}$ to isolate the known reference observatory position \mathbf{b} .

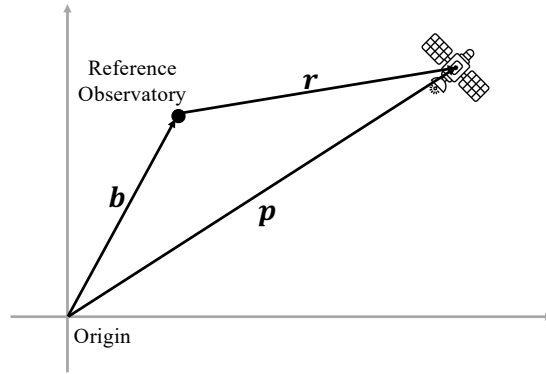


Fig. 8: The relation between the reference observatory position \mathbf{b} , spacecraft position \mathbf{p} , and the spacecraft's relative position to the observatory, \mathbf{r} .

The line-of-sight vectors $\hat{\mathbf{u}}_i$ are assumed to be fixed (no proper motion) and invariant for observers at different points in the Solar System. This assumption is justified because the δ Scuti stars considered in this study (shown in Table A1 and discussed later in the paper) have proper motion and annual parallaxes no greater than

450 mas/yr and 130 mas respectively. The line-of-sight pointing error θ is therefore within $1'' \approx 5 \times 10^{-6}$ rad. By the small angle approximation, a pointing error between the fixed line-of-sight vector $\hat{\mathbf{u}}_i$ and true line-of-sight vector $\hat{\mathbf{u}}_i^*$ yields an error in the left-hand-side term of Eq. (3) which is approximated by Eq. (4).

$$\hat{\mathbf{u}}_i \cdot \mathbf{p} - \hat{\mathbf{u}}_i^* \cdot \mathbf{p} = (\hat{\mathbf{u}}_i - \hat{\mathbf{u}}_i^*) \cdot \mathbf{p} = \sin \theta \cdot \|\mathbf{p}\| \approx \theta \cdot \|\mathbf{p}\| \quad (4)$$

For the error in the line of sight vector to be negligible, the error induced by ignoring line of sight changes must be much smaller than the uncertainty on the right-hand-side of Eq. (3), where the uncertainty in the estimate of T_i is σ_T . In other words, the following must hold:

$$\theta \cdot \|\mathbf{p}\| \ll c \cdot \sigma_T \Rightarrow 5 \times 10^{-6} \cdot \|\mathbf{p}\| < \frac{c \cdot \sigma_T}{100} \Rightarrow 1.67 \times 10^{-12} \cdot \|\mathbf{p}\| < \sigma_T \quad (5)$$

Therefore, the constant line of sight assumption is valid if $\sigma_T > 0.25$ s for $\|\mathbf{p}\| = 1$ au, and if $\sigma_T > 5$ s for $\|\mathbf{p}\| = 20$ au. For reference, σ_T values found for the case studies in the present analysis are typically on the order of 20 s.

Next, we obtain Eq. (6) by separating unknowns in Eq. (3) using $\mathbf{r} = \mathbf{p} - \mathbf{b}$.

$$\hat{\mathbf{u}}_i \cdot \mathbf{r} + c \cdot t = c \cdot T_i - \hat{\mathbf{u}}_i \cdot \mathbf{b} \quad (6)$$

Combining observations from multiple δ Scuti stars into a linear system then yields Eq. (7), whose constituents are defined in Eq. (8) and \mathbf{n} is the noise vector in measuring \mathbf{d} due to the uncertainty in T_i . Here, $\mathbf{A} \in \mathbb{R}^{N \times 4}$; $\{\mathbf{s}, \mathbf{d}, \mathbf{n}\} \in \mathbb{R}^4$.

$$\mathbf{A} \mathbf{s} = \mathbf{d} + \mathbf{n} \quad (7)$$

$$\mathbf{A} = \begin{bmatrix} \mathbb{1}_N, \begin{bmatrix} \hat{\mathbf{u}}_1^\top \\ \vdots \\ \hat{\mathbf{u}}_N^\top \end{bmatrix} \end{bmatrix}, \mathbf{s} = \begin{bmatrix} c \cdot t \\ \mathbf{r} \end{bmatrix}, \mathbf{d} = \begin{bmatrix} c \cdot T_1 - \hat{\mathbf{u}}_1 \cdot \mathbf{b} \\ \vdots \\ c \cdot T_N - \hat{\mathbf{u}}_N \cdot \mathbf{b} \end{bmatrix} \quad (8)$$

Assuming that the timing estimates $\{T_1, \dots, T_N\}$ have covariance matrix $\mathbf{\Omega}_T$, the covariance matrix of \mathbf{d} is then $\mathbf{\Omega}_d = c^2 \mathbf{\Omega}_T$. Define $\mathbf{W} = \mathbf{\Omega}_d^{-1}$. Here, $\{\mathbf{W}, \mathbf{\Omega}_T, \mathbf{\Omega}_d\} \in \mathbb{R}^{N \times N}$. The closed-form weighted least-squares solution to Eq. (7) is then:

$$\mathbf{s}^* = (\mathbf{A}^\top \mathbf{W} \mathbf{A})^{-1} \mathbf{A}^\top \mathbf{W} \mathbf{d}. \quad (9)$$

This means that a space and time solution can be found given pulsation models of a set of δ Scuti stars ($\omega_b(t)$) and signal time of arrival estimates at the reference observatory (T). Recall that in a lost in space and time scenario there are multiple estimates of T for each star, so each estimate of T would produce a different solution for \mathbf{s}^* . A method for resolving the ambiguity in T is presented in the following subsection.

5.2 Search Algorithm for Ambiguity Resolution

Hou presented an algorithm for ambiguity resolution in the context of X-ray pulsar navigation, which allows the concept in Figure 7 to be performed efficiently [9]. Given a convex, three-dimensional spatial search region, the algorithm updates a position solution by incrementally incorporating wavefronts from more pulsars. In this paper, the algorithm is adapted to δ Scuti stars in four-dimensional spacetime and summarized in Algorithm 1.

The algorithm assumes a convex four-dimensional search region. If the spacecraft state and uncertainty is known at a prior time, it is possible to propagate the spacecraft uncertainty to generate the search region. If the spacecraft state is unknown, the search region can simply be the entire Solar System. A non-convex region can be partitioned into several smaller, convex regions for which the algorithm can be applied.

Nonlinear dynamics such as proper motion, the parallax effect, and wavefront distortions due to relativistic effects are omitted because their impact on timing accuracy is negligible compared to measurement uncertainty. In other words, it is assumed that the wavefronts are planar and parallel.

Algorithm 1 An ambiguity resolution algorithm for identifying spacecraft time and position from δ Scuti star light curve observations.

```

1: function CANDIDATE_SEARCH( $i, \tilde{\mathbf{s}}, \mathbf{d}$ )
2:    $\{c \cdot \tilde{t}, \tilde{\mathbf{r}}\} \leftarrow \tilde{\mathbf{s}}$ 
3:   if  $i < 4$  then  $\triangleright$  Local minima of the light curve fit.
4:      $\tau_i \leftarrow \{T \mid J'(T) = 0, J''(T) > 0\}$ 
5:   else  $\triangleright$  Wavefronts near the existing solution.
6:      $\tau_i \leftarrow \{T \mid J'(T) = 0, J''(T) > 0, |c \cdot T - \hat{\mathbf{u}}_i \cdot \tilde{\mathbf{r}} - c \cdot \tilde{t}| < 9\sigma_{T_i}\}$ 
7:   loop
8:      $T_i \leftarrow \text{NEXT}(\tau_i)$   $\triangleright$  Iterate through each value in  $\tau_i$ .
9:      $d_i \leftarrow c \cdot T_i - \hat{\mathbf{u}}_i \cdot \mathbf{b}$ 
10:    if  $i \geq 4$  then
11:       $\triangleright A_{ii}$  is full rank, compute weighted least-squares solution.  $\triangleleft$ 
12:       $\mathbf{A}_{ii} \leftarrow \mathbf{A}[1 : i, 1 : i]$ 
13:       $\mathbf{W}_{ii} \leftarrow \mathbf{W}[1 : i, 1 : i]$ 
14:       $\tilde{\mathbf{s}} \leftarrow (\mathbf{A}_{ii}^\top \mathbf{W}_{ii} \mathbf{A}_{ii})^{-1} \mathbf{A}_{ii}^\top \mathbf{W}_{ii} \mathbf{d}[1 : i]$ 
15:      if  $\tilde{\mathbf{s}}$  outside search domain then continue
16:      if  $\mathbf{A}_{ii} \tilde{\mathbf{s}} - \mathbf{d}[1 : i]$  exceeds error bounds then continue
17:    if  $i < N$  then
18:       $\triangleright$  Include more  $\delta$  Scuti stars.  $\triangleleft$ 
19:      CANDIDATE_SEARCH( $i + 1, \tilde{\mathbf{s}}, \mathbf{d}$ )
20:    else
21:       $\text{store } \tilde{\mathbf{s}}$   $\triangleright$  All  $\delta$  Scuti star observations used. Record valid solution.

```

6 Feasibility Assessment

We performed error analysis for the proposed navigation algorithm using Monte Carlo simulation with the OSIRIS-APEX trajectory and MapCam detector parameters. First, a nominal observation scenario is considered. Then, the effects of varying observation conditions are explored.

6.1 Nominal Case

Monte Carlo simulations are used to assess the feasibility of obtaining a position and time solution through optical observations of δ Scuti stars. The spacecraft (OSIRIS-APEX) is assumed to be lost in space and time at MJD 60555.0; the position of the spacecraft is known to be contained within a three-dimensional sphere of radius 40 au; the current time is known to be contained within a range of ± 12 days; the attitude of the spacecraft is assumed to be known through star tracker observations [35].

Using the light curve simulation method described in Section 4, 11 δ Scuti stars are sequentially observed and wavefronts are computed for each star. The light curve simulation result from one Monte Carlo instance was shown in Figure 5. The time and position of the spacecraft is computed using Algorithm 1.

Figure 9 shows the result of a 1000-sample Monte Carlo simulation with the above conditions. The time estimate error has mean 1.7 s and standard deviation 4.7 s. The position estimate error has mean 1.8×10^{-2} au and standard deviation 1.6×10^{-2} au. Of the 1000 Monte Carlo instances, 964 succeeded in finding the spacecraft coordinate, while the remaining 36 cases produced no solution.

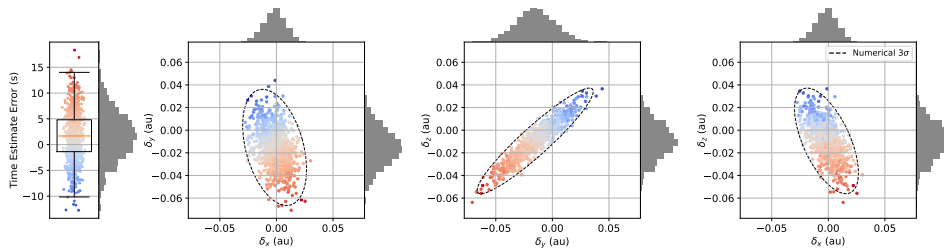


Fig. 9: Time and position error distribution for a 1000-sample Monte Carlo simulation of the proposed navigation method using 11 δ Scuti stars. The search radius is 12 days and 40 au. The numerical 3σ uncertainty ellipse is shown.

It should be noted that our method can accommodate search regions of far greater or smaller sizes, but more δ Scuti stars may need to be observed in order to resolve

ambiguity in a larger search space. Additionally, the compute time increases linearly with respect to the four-dimensional volume of the search region. Solving 1000 Monte Carlo instances takes less than 5 seconds on an Apple M2 CPU (single-threaded performance).

6.2 Parameterized Study

The effect of changing observation parameters on the position and time error of the proposed navigation method is analyzed using Monte Carlo simulation, with results shown in Table 3. Parameters considered include the observation time spent on each star, the cadence of observations, the exposure time for each observation, and the number of repetitions — meaning how many times the sequential observation of all stars is repeated.

The scenario discussed in Section 6.1 is considered the nominal case and shown as Case 1 in the table. The position and time errors and uncertainty values are slightly different due to results in Table 3 using 300 Monte Carlo samples rather than 1000.

Table 3: Position and time solution error and uncertainty for varied observation parameters, based on 300-sample Monte Carlo simulation results.

#	Obsv. Time (hr/star/rep)	Exposure (s) / Cadence (s)	Reps	Position Error(1σ) (au)	Time Error(1σ) (s)	Success Rate
1	1.0	3.0 / 3.0	2	$2.55(1.54) \times 10^{-2}$	3.35(4.53)	1.000
2	1.0	1.5 / 3.0	2	$2.72(2.15) \times 10^{-2}$	3.79(6.20)	1.000
3	1.0	0.5 / 3.0	2	$2.88(3.73) \times 10^{-2}$	3.92(11.30)	0.973
4	1.0	1.5 / 1.5	2	$2.88(1.75) \times 10^{-2}$	3.68(4.68)	1.000
5	1.0	6.0 / 6.0	2	$2.35(1.61) \times 10^{-2}$	2.52(4.69)	1.000
6	0.5	3.0 / 3.0	2	N/A	N/A	0
7	0.67	3.0 / 3.0	2	$1.72(1.45) \times 10^{-2}$	1.95(5.11)	1.000
8	1.5	3.0 / 3.0	2	$2.45(1.31) \times 10^{-2}$	0.12(3.39)	1.000
9	1.0	3.0 / 3.0	3	$4.30(1.49) \times 10^{-2}$	6.54(3.49)	1.000
10	1.0	3.0 / 3.0	4	$4.30(1.22) \times 10^{-2}$	4.78(2.74)	1.000
11	1.0	3.0 / 3.0	5	$3.92(1.09) \times 10^{-2}$	1.76(2.40)	1.000
12	0.67	3.0 / 3.0	3	$4.95(1.39) \times 10^{-2}$	7.29(4.13)	1.000
13	0.5	3.0 / 3.0	3	$1.31(1.73) \times 10^{-2}$	0.56(5.05)	1.000
14	0.5	6.0 / 6.0	4	$1.58(1.56) \times 10^{-2}$	0.69(3.98)	0.997

From Cases 1, 2, and 3, the solution variance scales proportionally to the inverse of exposure time for a fixed cadence. This is likely due to longer exposure images having a higher SNR, which in turn allows T , the position of δ Scuti star wavefronts, to be estimated with greater accuracy.

Comparing Cases 1, 4, and 5 suggests that lengthening cadences to allow even longer exposure times only marginally reduces mean solution error. Slowing down the imaging cadence reduces the total number of data points available to fit the δ Scuti star light curve, so although each individual flux measurement is more accurate, the estimate of the wavefront position doesn't change substantially.

In Cases 6-13, the total observation time (obsv. time \times # of stars \times repetitions) is varied by adjusting the observation time per star and/or the number of repetitions. If the total observation time is increased, more data is available to develop better estimates of the wavefronts. However, the spacecraft will have traveled a greater distance which is not accounted for in the proposed solution, so there will be a greater bias in the position and time estimate. For example, in Cases 9-11 the position uncertainty decreases but the mean position error is largely unchanged, so the 3σ error ellipse no longer overlaps the true solution.

Conversely, reducing the total observation time may slightly decrease solution errors due to the smaller amount of spacecraft motion as with Cases 7 and 13, but too little observation time may cause wavefront estimation and the navigation algorithm to fail such as in Case 6. Finally, given a fixed total observation time, it is unclear whether it is better to prioritize longer observations per star or number of repetitions. While Case 1 vs. 12 or Case 8 vs. 9 indicate that prioritizing longer observations per star is better, Case 5 vs. 14 suggests otherwise.

We emphasize that the present study only explores the impact of variations in broadly applicable observation parameters through the lens of OSIRIS-APEX and

MapCam. Other important factors, such as sensor parameters and calibration, spacecraft trajectory, and specific δ Scuti stars selected for navigation, may also heavily affect navigation accuracy and must be assessed on a per-mission basis. Nonetheless, our findings suggest that autonomous recovery from being lost in space and time may be feasible using existing spacecraft instruments with our proposed method.

7 Conclusions

A method for solving the lost in space and time problem using optical observations of δ Scuti stars is developed. The feasibility of the method is explored with consideration for detector performance constraints, δ Scuti star pulsation models, and spacecraft motion. Case studies indicate that it may be possible to for OSIRIS-APEX to recover position and time information using MapCam observations of δ Scuti stars alone to accuracies within 0.05 au (3σ) and 15 s (3σ), respectively.

Acknowledgements. This paper includes data collected by the TESS mission. Funding for the TESS mission is provided by the NASA’s Science Mission Directorate.

Appendix A δ Scuti Stars within Visibility Criteria

Table A1: List of δ Scuti stars with $m_V < 7.0$, $\Delta V > 0.04$ mag, and $P < 0.20$ d.

Name	Max (Vmag)	Amplitude (Vmag)	Period (d)	RA (deg)	DEC (deg)
V0474 Mon	5.94	0.370	0.136	89.754	-9.382
rho Pup	2.68	0.190	0.141	121.886	-24.304
V0376 Per	5.77	0.140	0.099	57.284	43.963
IM Tau	5.33	0.130	0.145	62.708	26.481
VX Psc	5.90	0.120	0.131	22.470	18.356

Table A1 continued.

Name	Max (Vmag)	Amplitude (Vmag)	Period (d)	RA (deg)	DEC (deg)
del Del	4.38	0.110	0.157	310.865	15.075
bet Cep	3.16	0.110	0.190	322.165	70.561
WZ Scl	6.52	0.100	0.096	22.181	-33.764
VY Crt	6.85	0.100	0.136	175.492	-24.386
BV Cir	6.80	0.100	0.158	225.259	-64.576
X Cae	6.28	0.100	0.135	76.109	-35.705
tet Tuc	6.06	0.090	0.049	8.347	-71.266
V0784 Cas	6.61	0.090	0.109	32.606	59.980
AI CVn	5.99	0.090	0.116	185.946	42.543
HT Peg	5.30	0.090	0.060	358.155	10.947
FM Vir	5.20	0.080	0.072	191.404	7.673
V0386 Per	6.50	0.080	0.052	59.513	34.814
WW LMi	6.16	0.070	0.127	163.676	25.491
AZ CMi	6.44	0.070	0.095	116.032	2.405
eta Hya	4.27	0.060	0.170	130.806	3.399
V0696 Tau	5.22	0.060	0.036	65.151	15.095
gam CrB	3.80	0.060	0.030	235.686	26.296
BT Cnc	6.66	0.060	0.102	129.928	19.778
CC Gru	6.62	0.060	0.126	339.785	-52.692
rho Pav	4.85	0.055	0.114	309.397	-61.530
GN And	5.23	0.050	0.069	7.531	29.752
sig Oct	5.45	0.050	0.097	317.195	-88.957
EN UMa	5.83	0.050	0.155	155.264	68.748
DK Vir	6.67	0.050	0.119	199.106	-1.391

Table A1 continued.

Name	Max (Vmag)	Amplitude (Vmag)	Period (d)	RA (deg)	DEC (deg)
V0637 Mon	4.96	0.050	0.191	105.728	-4.239
del Cet	4.05	0.050	0.161	39.871	0.329
LW Vel	5.24	0.050	0.111	153.345	-51.233
iot Boo	4.73	0.050	0.027	214.041	51.367
FG Vir	6.53	0.050	0.079	183.564	-5.717
V1208 Aql	5.51	0.050	0.150	289.914	12.375
AO CVn	4.70	0.050	0.122	199.386	40.573
alf Mus	2.68	0.050	0.090	189.296	-69.136
del Lup	3.20	0.040	0.165	230.343	-40.648
tau 1 Lup	4.54	0.040	0.177	216.534	-45.221
UV Ari	5.18	0.040	0.035	41.240	12.446
HD 46089	5.21	0.040	0.050	97.951	11.544
bet Cas	2.25	0.040	0.101	2.295	59.150
V1004 Ori	5.88	0.040	0.061	89.602	1.837
V0620 Her	6.19	0.040	0.080	257.763	24.238

References

- [1] Fountain, G.H., Kusnierkiewicz, D.Y., Hersman, C.B., Herder, T.S., Coughlin, T.B., Gibson, W.C., Clancy, D.A., DeBoy, C.C., Hill, T.A., Kinnison, J.D., *et al.*: The New Horizons Spacecraft. *Space science reviews* **140**, 23–47 (2008) <https://doi.org/10.1007/s11214-008-9374-8>
- [2] Ecale, E., Torelli, F., Tanco, I.: JUICE interplanetary operations design: drivers and challenges. In: 2018 SpaceOps Conference, p. 2493 (2018). <https://doi.org/>

[10.2514/6.2018-2493](https://doi.org/10.2514/6.2018-2493)

- [3] Keil, J., Herfort, U.: Contingency Operations during Failure of Inertial Attitude Acquisition Due to Star Tracker Blinding for Three-Axes-Stabilized Interplanetary Spacecraft. In: Proceedings of the 20th International Symposium on Space Flight Dynamics (2007). <https://ntrs.nasa.gov/citations/20080012644>
- [4] Cox, M.W., Ossing, D.A.: The fall and rise of stereo behind. In: 2018 SpaceOps Conference, p. 2565 (2018). <https://doi.org/10.2514/6.2018-2565>
- [5] Jet Propulsion Laboratory: NASA Mission Update: Voyager 2 Communications Pause. <https://www.jpl.nasa.gov/news/nasa-mission-update-voyager-2-communications-pause> [Accessed Jan. 10, 2024] (2023)
- [6] Johnston, M.D.: Scheduling NASA’s Deep Space Network: Priorities, Preferences, and Optimization. In: ICAPS - SPARK Workshop. JPL Open Repository, ??? (2020). <https://hdl.handle.net/2014/53269>
- [7] Tanygin, S.: Closed-form solution for lost-in-space visual navigation problem. *Journal of Guidance, Control, and Dynamics* **37**(6), 1754–1766 (2014) <https://doi.org/10.2514/1.G000529>
- [8] Hollenberg, C.L., Christian, J.A.: Geometric solutions for problems in velocity-based orbit determination. *The Journal of the Astronautical Sciences* **67**(1), 188–224 (2020) <https://doi.org/10.1007/s40295-019-00170-7>
- [9] Hou, L., Putnam, Z.R.: A norm-minimization algorithm for solving the lost-in-space problem with xnav. *The Journal of the Astronautical Sciences* **71**(1), 6 (2024) <https://doi.org/10.1007/s40295-023-00425-4>

- [10] Adams, V.H., Peck, M.A.: Lost in space and time. In: AIAA Guidance, Navigation, and Control Conference, p. 1030 (2017). <https://doi.org/10.2514/6.2017-1030>
- [11] Dahir, A.R.: Lost in space: Autonomous deep space navigation. PhD thesis, University of Colorado at Boulder (2020). <https://www.proquest.com/docview/2408808776>
- [12] Sala Álvarez, J., Urruela Planas, A., Villares Piera, N.J.: Feasibility study for a spacecraft navigation system relying on pulsar timing information (2004). https://upcommons.upc.edu/bitstream/handle/2117/11514/final_report_23062004.pdf
- [13] Eyer, L., Mowlavi, N.: Variable stars across the observational hr diagram. In: Journal of Physics: Conference Series, vol. 118, p. 012010 (2008). <https://doi.org/10.1088/1742-6596/118/1/012010> . IOP Publishing
- [14] Aerts, C., Christensen-Dalsgaard, J., Kurtz, D.W.: 3. Asteroseismology. Springer, ??? (2010)
- [15] Handler, G.: Delta scuti variables. In: AIP Conference Proceedings, vol. 1170, pp. 403–409 (2009). <https://doi.org/10.1063/1.3246528> . American Institute of Physics
- [16] Watson, C.L., Henden, A.A., Price, A.: The international variable star index (vsx). In: The Society for Astronomical Sciences 25th Annual Symposium on Telescope Science. Held May 23-25, 2006, at Big Bear, CA. Published by the Society for Astronomical Sciences., P. 47, vol. 25, p. 47 (2006)
- [17] Mantegazza, L., Zerbi, F.M., Sacchi, A.: Simultaneous intensive photometry and high resolution spectroscopy of delta scuti stars iv. an improved picture of the pulsational behaviour of x caeli. arXiv preprint astro-ph/9911337 (1999) <https://arxiv.org/abs/astro-ph/9911337>

[//doi.org/10.48550/arXiv.astro-ph/9911337](https://doi.org/10.48550/arXiv.astro-ph/9911337)

- [18] Rizk, B., Drouet d'Aubigny, C., Golish, D., Fellows, C., Merrill, C., Smith, P., Walker, M., Hendershot, J., Hancock, J., Bailey, S., *et al.*: Ocams: the osiris-rex camera suite. *Space Science Reviews* **214**, 1–55 (2018) <https://doi.org/10.1007/s11214-017-0460-7>
- [19] Golish, D., Drouet d'Aubigny, C., Rizk, B., DellaGiustina, D., Smith, P., Becker, K., Shultz, N., Stone, T., Barker, M., Mazarico, E., *et al.*: Ground and in-flight calibration of the osiris-rex camera suite. *Space science reviews* **216**, 1–31 (2020) <https://doi.org/10.1007/s11214-019-0626-6>
- [20] Bos, B., Nelson, D., Pelgrift, J., Liounis, A., Doelling, D., Norman, C., Olds, R., May, C., Witherspoon, R., Church, E., *et al.*: In-flight calibration and performance of the osiris-rex touch and go camera system (tagcams). *Space Science Reviews* **216**, 1–52 (2020) <https://doi.org/10.1007/s11214-020-00682-x>
- [21] Blue Canyon Technologies Components. <https://bluecanyontech.com/components>. Accessed: 2023-08-28
- [22] Space Micro muSTAR Star Tracker Datasheets. Accessed: 2023-08-28
- [23] Terma T1 Star Tracker Datasheet. Accessed: 2023-08-28
- [24] Rowen, D., Pralle, M., Utter, A., Kinum, G., Weiher, H., Wu, A., Dolphus, R., Alcid, E.: On-orbit results from an ultra-low swap black silicon star tracker. In: 34th Annual Small Satellite Conference (2020). <https://digitalcommons.usu.edu/cgi/viewcontent.cgi?article=4766&context=smallsat>
- [25] Huffman, K., Sedwick, R., Stafford, J., Peverill, J., Seng, W.: Designing star trackers to meet micro-satellite requirements. In: SpaceOps 2006 Conference, p.

- 5654 (2006). <https://doi.org/10.2514/6.2006-5654>
- [26] XQE CMOS Sensor Datasheet. http://www.micronkk.com/0_datalibrary/sionyx/XQE-0920_en.pdf. Accessed: 2023-08-28
- [27] Erlank, A.O.: Development of cubestar: a cubesat-compatible star tracker. PhD thesis, Stellenbosch: Stellenbosch University (2013). <https://core.ac.uk/download/pdf/37420644.pdf>
- [28] CubeSpace CubeStar Gen 1 Specifications. <https://www.cubespace.co.za/products/gen-1/sensors/cubestar/>. Accessed: 2023-08-28
- [29] Kruger, J., D’Amico, S.: Autonomous angles-only multitarget tracking for spacecraft swarms. *Acta Astronautica* **189**, 514–529 (2021) <https://doi.org/10.1016/j.actaastro.2021.08.049>
- [30] ONSemi HAS2 Image Sensor Datasheet. Accessed: 2023-08-28
- [31] Ogiers, W., Ruythooren, K., Van Wichelen, K., Dendoncker, M., Kowaltschek, S., Razgus, B.: Faintstar: an intelligent single-chip sensor head for star trackers—prototype results. *CEAS Space Journal* **10**, 605–619 (2018) <https://doi.org/10.1007/s12567-018-0220-x>
- [32] Fillfactory CMOS Image Sensor IBIS5-A-1300 Datasheet. Accessed: 2023-08-28
- [33] Sheikh, S.I., Hanson, J.E., Graven, P.H., Pines, D.J.: Spacecraft navigation and timing using x-ray pulsars. *Navigation* **58**(2), 165–186 (2011) <https://doi.org/10.1002/j.2161-4296.2011.tb01799.x>
- [34] Lohan, K.: Methodology for state determination without prior information using x-ray pulsar navigation systems. PhD thesis, University of Illinois at Urbana-Champaign (2021). <https://hdl.handle.net/2142/113068>

- [35] Rijlaarsdam, D., Yous, H., Byrne, J., Oddenino, D., Furano, G., Moloney, D.: A survey of lost-in-space star identification algorithms since 2009. *Sensors* **20**(9), 2579 (2020) <https://doi.org/10.3390/s20092579>